Ab initio molecular dynamics of hydrogen dissociation on metal surfaces using neural networks and novelty sampling

Jeffery Ludwig and Dionisios G. Vlachos

Citation: The Journal of Chemical Physics **127**, 154716 (2007); doi: 10.1063/1.2794338
View online: http://dx.doi.org/10.1063/1.2794338
View Table of Contents: http://aip.scitation.org/toc/jcp/127/15
Published by the American Institute of Physics

Ab initio molecular dynamics of hydrogen dissociation on metal surfaces using neural networks and novelty sampling

Jeffery Ludwig and Dionisios G. Vlachos[a)]
Department of Chemical Engineering and Center for Catalytic Science and Technology, University of Delaware, Newark, Delaware 19716-3110, USA

(Received 2 February 2007; accepted 12 September 2007; published online 18 October 2007)

We outline a hybrid multiscale approach for the construction of *ab initio* potential energy surfaces (PESs) useful for performing six-dimensional (6D) classical or quantum mechanical molecular dynamics (MD) simulations of diatomic molecules reacting at single crystal surfaces. The algorithm implements concepts from the corrugation reduction procedure, which reduces energetic variation in the PES, and uses neural networks for interpolation of smoothed *ab initio* data. A novelty sampling scheme is implemented and used to identify configurations that are most likely to be predicted inaccurately by the neural network. This hybrid multiscale approach, which couples PES construction at the electronic structure level to MD simulations at the atomistic scale, reduces the number of density functional theory (DFT) calculations needed to specify an accurate PES. Due to the iterative nature of the novelty sampling algorithm, it is possible to obtain a quantitative measure of the convergence of the PES with respect to the number of *ab initio* calculations used to train the neural network. We demonstrate the algorithm by first applying it to two analytic potentials, which model the H_2/Pt(111) and H_2/Cu(111) systems. These potentials are of the corrugated London-Eyring-Polanyi-Sato form, which are based on DFT calculations, but are not globally accurate. After demonstrating the convergence of the PES using these simple potentials, we use DFT calculations directly and obtain converged semiclassical trajectories for the H_2/Pt(111) system at the PW91/generalized gradient approximation level. We obtain a converged PES for a 6D hydrogen-surface dissociation reaction using novelty sampling coupled directly to DFT. These results, in excellent agreement with experiments and previous theoretical work, are compared to previous simulations in order to explore the sensitivity of the PES (and therefore MD) to the choice of exchange and correlation functional. Despite having a lower energetic corrugation in our PES, we obtain a broader reaction probability curve than previous simulations, which is attributed to increased geometric corrugation in the PES and the effect of nonparallel dissociation pathways.
 [DOI: 10.1063/1.2794338]

I. INTRODUCTION

Quantum dynamics simulations using a potential energy surface (PES) based entirely on density functional theory (DFT) calculations have allowed unprecedented insight into the dynamics of the dissociation of diatomic molecules at metal surfaces.[1–4] Specifically, the dissociative adsorption of hydrogen on Pt(111) has been studied extensively both experimentally[5–8] and theoretically[7,9–22] due to its importance as an elementary step in many industrially relevant catalytic processes. Because of the low energetic barriers encountered during dissociation (1.4–9.7 kcal/mol depending on dissociation site)[20] and the presence of multiple reaction channels, molecular dynamics (MD) simulations using a reactive force field are an invaluable tool in understanding the physics of this process. Recently, six-dimensional (6D) quantum dynamics simulations have been able to resolve two apparently conflicting experiments on the H_2/Pt(111) system.[7,20] Theoretical results indicated that the PES was energetically corrugated, in agreement with molecular beam experiments,[6,8] and that this corrugation was not seen in diffraction experiments[5] since only in-plane diffraction was studied. It was suggested that the energetic corrugation in the PES would only manifest itself in out-of-plane diffraction, which was subsequently confirmed by experiments.[7]

As a model system for studying surface dynamics, H_2/Pt(111) is in many ways ideal. There are two independent sets of experimental data for the dissociation reaction,[6,8] the system exhibits no isotope effect,[6,22] the large size difference between hydrogen and platinum eliminates surface temperature effects,[6,22] the system is electronically adiabatic during reaction,[7] and a semiclassical treatment of dynamics has been shown to be in good agreement with a more accurate quantum dynamical approach.[21] However, the success of any atomistic simulation relies entirely on an accurate and realistic parametrization of a PES, which remains the key challenge in simulating these systems.

The most common approach used in recent literature for the construction of 6D PESs is the corrugation reduction procedure (CRP).[23] In this method, energetic variation in the PES is removed by subtracting corrugation due to the three-dimensional (3D) atom-surface interactions. A symmetry

[a)]Author to whom correspondence should be addressed. Electronic mail: vlachos@udel.edu

adapted interpolation is then performed on a smoothed database of potential energies. This approach, while powerful and successful, requires input data for the interpolation scheme to fall on a regular grid, which precludes the ability to add arbitrary configurations to the training set.

Crespos *et al.*[10,11] later developed an "off-grid" approach, extending the modified Sheppard (MS) interpolation[24,25] to diatom-surface systems. A key feature of this method is that configurations sampled from MD trajectories are used to grow the *ab initio* database until convergence is achieved. This is possible with the MS approach, since the potential is expressed as a weighted average of a Taylor expansion about each configuration, and does not require the input data to be regularly spaced. Due to the improved sampling of configuration space, this approach required less than half of the number of configurations (approximately 1300) to obtain a converged PES that reproduced the CRP potential for the H_2/Pt(111).[10,11] However, the CRP potential was used in the place of direct DFT calculations since the MS method requires a Hessian calculation for each configuration in the interpolation database. The Hessian calculation is computationally expensive when an *ab initio* technique is used directly. A later study by Diaz *et al.*[26] demonstrated this technique using a "live" DFT potential for the N_2/Ru(0001) system.

Lorenz *et al.*[27,28] provided another off-grid interpolation method, which used neural networks as interpolating functions in place of the Taylor expansion in the MS scheme. This technique does not require second derivatives, and was robust enough to capture the dynamics of hydrogen dissociating over clean and sulfur poisoned Pd surfaces. Recently, a hybrid of these two off-grid techniques was proposed.[29] The novelty sampling scheme[24,25] from the MS approach was combined with neural networks to create a novelty sampling method which does not require second derivatives of the potential.[29] This technique was used to study the decomposition of vinyl bromide,[29] nanometric cutting of silicon,[29] and the dissociation of SiO_2.[30]

In this paper, we extend the neural network/novelty sampling approach to diatom-surface systems. Instead of using neural networks to model the entire potential energy, we first eliminate as much energetic variation in the PES as possible using a modified form of the CRP.[23] Neural networks are then used as an interpolating function on this database of smoothed "residual" energies. A novelty sampling approach[24,29] is used to couple configurations included in the interpolating database with the configuration space explored during the MD simulations. This iterative approach creates a framework for obtaining converged dynamics for a given choice of exchange and correlation functionals within DFT. As the number of configurations in the training database increases, we obtain a dynamic result that is unique to the functionals used in DFT and the assumptions inherent in the MD. This multiscale approach drastically reduces the number of quantum mechanical calculations necessary for the development of an *ab initio* PES, and also provides a systematic framework for addressing PES accuracy.

We first demonstrate the approach on two analytic PESs, corrugated London-Eyring-Polanyi-Sato (LEPS) potentials for the H_2/Pt(111) (Ref. 15) and H_2/Cu(111) (Ref. 31) systems. We also demonstrate the methodology using *ab initio* energies directly for the H_2/Pt(111) system using the PW91 functional.[32] We demonstrate the convergence of a 6D diatom-surface PES based on "live" DFT calculations, without the need to calculate second derivatives for each point in the interpolation database. Simulations using our converged PES are compared to semiclassical simulations performed by Pijper *et al.*,[21] who used different exchange and correlation functionals to generate the PES, and experimental data. We begin in Sec. II by providing details of our calculations, and go on demonstrate the approach outlined in Sec. II to three different systems in Sec. III.

II. COMPUTATIONAL METHODS

The fundamental problem in performing classical or quantum *ab initio* MD simulations is the computational cost associated with electronic structure calculations, which are required to obtain the forces acting on the nuclei. A single MD trajectory may need 10^6 or more force calculations, and obtaining reliable ensemble averages may require thousands of trajectories. This effectively eliminates "real-time" quantum mechanical calculations as a viable option for obtaining estimates of reaction rates. The approach taken herein, and in many previous works, is the creation of an offline database of configurations and energies using the Born-Oppenheimer approximation. The entries in this database are then interpolated during MD simulations. Major issues are the specification of an interpolating function, and the proper sampling of configurations in phase space to ensure that the interpolation is accurate at the level required by the MD simulations. The functional form used in this work is a hybrid approach, combining a modification to the CRP methodology developed by Busnengo *et al.*[23] with the use of neural networks as an interpolating function.[27–29,33] We begin by describing the details of our semiclassical MD simulations and the DFT calculations used throughout this work. Next, we describe the construction of our potential function and the use of neural networks to fit smoothed DFT calculations. We finish this section with details about neural network training and a novelty sampling scheme which identifies the correct region of phase space that should be used to train the neural networks.

A. Molecular dynamics (MD)

Estimates of reaction probability as a function of collision energy can be obtained for diatom-surface systems by performing semiclassical MD simulations. For the H_2/Pt(111) system, semiclassical trajectories have been shown to be in good agreement with a more accurate quantum mechanical treatment.[21] All trajectories were started with the center of mass (COM) of a hydrogen molecule located 4.5 Å above the Pt surface. At this distance, the contribution of the Pt surface to the forces acting on the H_2 molecule is negligible. At the start of every trajectory, the x-y position of the COM was chosen randomly in the 2×2 surface unit cell, as was the initial polar angle and azimuth of the H–H bond. The initial distance between the two hydro-

gen atoms was held fixed at an equilibrium bond length of 0.763 Å, determined by DFT using the same functionals and basis set as applied to the surface.

The only initial internal energy considered was that of the zero point energy, which accounts for the vibrational motion of the H_2 molecule in the $v=0$ state. A more thorough discussion of the effect of including this energy in classical dynamics simulations is given for the H_2/Pt(211) system by McCormack *et al.*[34] Unless otherwise specified, all trajectories were performed without any initial momentum parallel to the surface. The trajectories were integrated in time using a velocity Verlet algorithm[35] with a time step of 0.05 fs until one of two dynamic outcomes was observed. If the bond length of the hydrogen molecule exceeded 3.0 Å at any point during the simulation, the trajectory was considered dissociated. If the COM position in the z direction exceeded the starting position of 4.5 Å, the trajectory was considered reflected. The sticking probability reported in this work is the fraction of the total number of trajectories, which dissociate. For each incident energy considered in this work, 1000 trajectories were performed, which corresponds to a 95% confidence interval of ±3% at $s_0=0.5$, based on the recommendation of Agresti and Coull[36] for binomial distributions. During dynamics simulations, total energy was conserved to 0.1 meV, and trajectories could be integrated backward in time from their final state so that the initial positions of the hydrogen atoms were recovered to within 10^{-6} Å (based on the L2 norm of the starting position vectors).

B. DFT calculations

All DFT calculations were performed on a Pt(111) surface, periodic in the x and y directions, using the DACAPO code.[37,38] The system consisted of a 2×2 surface unit cell, four layers thick, with approximately 11 Å of vacuum space between slabs in the z direction. The top two layers of the slab were allowed to relax, whereas the bottom two layers were fixed at their bulk equilibrium position. The lattice constant used in this work was 4.03 Å, which was determined by minimizing the energy of bulk Pt. During all subsequent calculations done with hydrogen in the system, the slab was kept frozen in this relaxed state, and the wavefunction was restricted to a singlet state. The rigid substrate assumption can be justified by the fact that the trapping probability of hydrogen on a Pt(111) surface is insensitive to surface temperature.[6] The Kohn-Sham wavefunction was expanded in a plane wave basis set with a 350 eV cutoff energy. Vanderbilt ultrasoft pseudopotentials[39] were used to model the core electrons and the Brillouin zone was sampled using a $4\times4\times1$ Monkhorst-Pack[40] scheme. The PW91 functional[32] was used to account for the electron exchange and correlation energy.

C. Potential energy surface

A slab and two isolated hydrogen atoms in vacuum were taken as the reference state. The potential energy is

$$V(\mathbf{r}_1,\mathbf{r}_2)=E(\mathbf{r}_1,\mathbf{r}_2)-E^{\mathrm{slab}}-2E^{\mathrm{H}}, \tag{1}$$

where $E(\mathbf{r}_1,\mathbf{r}_2)$ is the total energy calculated from DFT, E^{slab} is the total energy of the slab without any hydrogen in the system, and E^{H} is the total energy of a hydrogen atom in the doublet state in the gas phase. Because of the rigid substrate approximation, $E(\mathbf{r}_1,\mathbf{r}_2)$ is only a function of the positions of the hydrogen atoms, $\mathbf{r}_1$ and $\mathbf{r}_2$. The potential energy for a given system configuration is broken down into pair-additive and non-pair-additive terms

$$V(\mathbf{r}_1,\mathbf{r}_2)=V^{\mathrm{H-H}}(\|\mathbf{r}_1-\mathbf{r}_2\|)+V^{\mathrm{Pt\text{-}1}}(\mathbf{r}_1)+V^{\mathrm{Pt\text{-}2}}(\mathbf{r}_2)+V^{\mathrm{NN}}(\mathbf{q}), \tag{2}$$

where V is the potential energy defined by Eq. (1), $V^{\mathrm{H-H}}$ is the potential energy of a hydrogen-hydrogen pair in the gas phase with no surface present, $V^{\mathrm{Pt\text{-}1}}$ is the potential energy of a single isolated hydrogen atom interacting with the surface, and $V^{\mathrm{Pt\text{-}2}}$ is the potential energy of a second isolated hydrogen atom interacting with the surface. The hydrogen-hydrogen potential is one dimensional and only a function of bond length, whereas the hydrogen-surface potential energy functions are 3D. V^{NN} is a residual term, which captures all non-pair-additive interactions in the system, and is discussed in more detail below. This separation of the total potential energy into pair-additive and non-pair-additive terms is similar to the CRP described by Busnengo *et al.*[23] The central concept behind this technique is that the majority of the energetic variation in the potential energy is due to variations in isolated atom-surface interactions. By subtracting out the pair-additive interactions, one is left with a much smoother function to interpolate over.

In addition to removing the atom-surface interactions, we also remove the atom-atom interactions. This ensures that V^{NN} tends to zero in the limits of configurations far away from the surface and infinite bond length. Far away from the surface, $V(\mathbf{r}_1,\mathbf{r}_2)\approx V^{\mathrm{H-H}}(\|\mathbf{r}_1-\mathbf{r}_2\|)$ and the potential reduces to a simple H–H pair potential. At very long bond lengths, $V(\mathbf{r}_1,\mathbf{r}_2)\approx V^{\mathrm{Pt\text{-}1}}(\mathbf{r}_1)+V^{\mathrm{Pt\text{-}2}}(\mathbf{r}_2)$, i.e., the system behaves like two noninteracting hydrogen atoms adsorbed on a surface. However, due to long-range adsorbate-adsorbate interactions, V^{NN} is not exactly zero when the bond length becomes moderately large (e.g., 3 Å). Figure 1 shows the contours of V and V^{NN} for the same two-dimensional slice of the full 6D PES. The largest values of V^{NN} are encountered in the elbow region of the plot, while the correction is much smaller far away from the surface, and at extended bond lengths.

The hydrogen-hydrogen pair potential, $V^{\mathrm{H-H}}$, is a modified Morse potential that was previously described.[15] The hydrogen-surface pair potentials are corrugated modified Morse potentials, similar to that used in other works,[15,23,31] but with slightly different basis functions and coefficients (see Appendix A).

The residual term, $V^{\mathrm{NN}}(\mathbf{q})$, is an interpolating function, in this case a neural network, which accounts for the potential energy's deviations from the pair-additive sum. The neural network takes a symmetry adapted coordinate as input, $\mathbf{q}$, which is described next. The structure and training of the neural network are also described below.

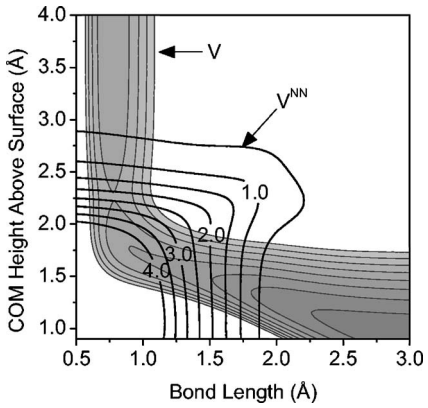

FIG. 1. V and V^{NN} contours for a two-dimensional slice of the corrugated LEPS PES which models the H_2/Pt(111) system. The two-dimensional cut is taken with the center of mass (COM) of the hydrogen molecule centered over a top site on the Pt(111) surface, and the H–H bond parallel to the surface. The two hydrogen atoms are oriented so that one is dissociating into an hcp hollow site, and the other hydrogen atom is dissociating into a fcc hollow site. Gray filled contour is the total potential energy, V, and is shown only for heights and bond length combinations that are likely to be encountered in MD simulations. The overlay of thick labeled lines represents, V^{NN}, each contour level representing 0.5 eV.

D. Coordinate system

The Cartesian coordinates for the two hydrogen atoms, $\mathbf{r}_1$ and $\mathbf{r}_2$, are not used directly as inputs to the interpolating function V^{NN}. Rather, a transformed coordinate $\mathbf{q}=q(\mathbf{r}_1,\mathbf{r}_2)$ is used that automatically accounts for the symmetry and periodicity of the fcc(111) surface. All recent methods of 6D PES development, CRP,[23] MS,[10,11] and neural networks,[27,28] explicitly account for surface symmetry using a similar approach. The transformation used in this work is valid for fcc(111) and hcp(0001) systems, and is based on the first few terms of a Fourier series

$$\mathbf{q}=\begin{bmatrix} \cos(2\alpha y_1/\sqrt{3})+2\cos(\alpha x_1)\cos(\alpha y_1/\sqrt{3}) \\ \sin(2\alpha y_1/\sqrt{3})-2\cos(\alpha x_1)\sin(\alpha y_1/\sqrt{3}) \\ z_1 \\ \cos(2\alpha y_2/\sqrt{3})+2\cos(\alpha x_2)\cos(\alpha y_2/\sqrt{3}) \\ \sin(2\alpha y_2/\sqrt{3})-2\cos(\alpha x_2)\sin(\alpha y_2/\sqrt{3}) \\ z_2 \\ \|\mathbf{r}_1-\mathbf{r}_2\| \end{bmatrix}, \tag{3}$$

where x_i, y_i, and z_i are the x, y, and z coordinates for atom i, $\|\mathbf{r}_1-\mathbf{r}_2\|$ is the molecule's bond length, and α is a constant related to the lattice constant a_0 via

$$\alpha=\frac{2\pi}{\sqrt{2}a_0}. \tag{4}$$

The first and second terms of $\mathbf{q}$ are the first nontrivial even and odd terms of a Fourier series based on reciprocal lattice vectors of the fcc(111) 2×2 surface, grouped to maintain C_{3v} symmetry. The fourth and fifth terms are identical to the first two terms, except that they refer to the second hydrogen atom in the system. By explicitly introducing the correct symmetry into the coordinate system, we eliminate the need to include symmetric configurations via a "brute force" process. In a brute force approach, one would take each configuration in the training database and find equivalent configurations in the surface unit cell by applying a series of mirror, rotation, and translation operations. For example, a fcc(111) 2×2 surface unit cell with a heteronuclear diatomic molecule would require five additional mirror configurations in the training database to properly account for symmetry. However, using the coordinate transform of Eq. (3), all six of these configurations have the same $\mathbf{q}$ vector. By eliminating the need to include equivalent configurations due to symmetry, the neural network training database is reduced by a factor of 6. Without this reduction, neural network training time would be increased by two orders of magnitude, and become more time consuming than the DFT calculations needed to generate the training database.

E. Neural network

The use of a neural network as a general interpolation tool for PESs is well established.[27–30,33,41–51] The advantages over other interpolation techniques include well developed commercial toolboxes,[52] good scaling with system dimensionality, and ease of handling irregularly spaced data. The approach outlined here closely follows the extension to diatomic-single crystal systems by Lorenz *et al.*[27,28] We refer the reader to Ref. 52 for a more general description of neural network terminology, implementation details, and training algorithms. An important difference between this work and that of Lorenz *et al.*[27,28] is that we use the neural networks only for the residual term in Eq. (2), as opposed to the entire potential. With much of the energetic variation removed, the network is given a smoother dataset to interpolate over, which reduces training time and gives the potential the correct limiting behavior.

The neural network used in this work has a feedforward structure with one hidden layer. The input layer of the neural network uses a logsig transfer function, the hidden layer uses a tansig transfer function, and the output layer uses a linear transfer function. In the notation of Blank *et al.*,[33] we use networks of the *N-M-1 stl* form, N representing the number of neurons in the input layer, and M representing the number of neurons in the hidden layer. The output layer has a size of 1 since the neural network outputs a scalar value, the potential energy. Prior to network training, the inputs and targets of the neural network undergo a significant amount of preprocessing. While the transformed coordinate system of Eq. (3) accounts for mirror symmetry in the system, it does not account for exchange symmetry in the case of a homonuclear diatomic. For every $\mathbf{q}$ vector in the training set, its mirror image was added to the database by exchanging the first three elements of $\mathbf{q}$ with the fourth through sixth elements (the seventh element, bond length, remains the same).

The network inputs, now twice as numerous due to exchange symmetry, were linearly scaled so that they have zero mean, and unit standard deviation. The network targets, $V^{NN}(\mathbf{q}_i)$, were also scaled linearly so that they fell on the interval $[-1,1]$. This scaling is done to improve network training,[52] as it causes the inputs and outputs to fall within ranges where the transfer functions have a lot of activity.

The network was trained using the MATLAB neural net-

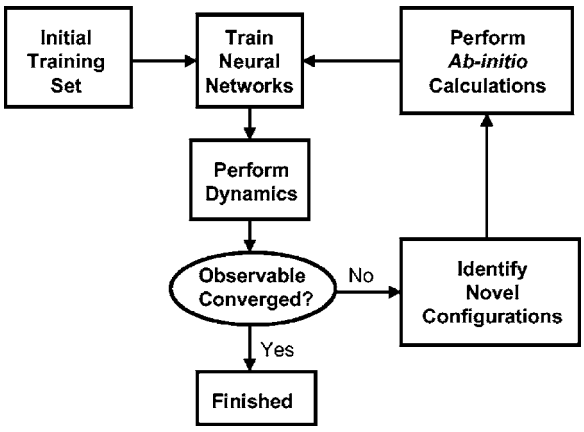

FIG. 2. Novelty sampling algorithm followed to obtain a converged potential energy surface.

work toolbox,[52] using the Levenberg-Marquardt minimization procedure,[53] and early stopping.[54] Prior to network training, the data were randomly divided in an 80/20 ratio into training and validation sets, the latter of which was used to trigger the early stopping process. The validation set was not used to generate any gradient information during the Levenberg-Marquardt minimization procedure. Network size was held symmetric ($N=M$) and chosen so that no further improvement in the fit of training or validation sets was obtained. For every database considered in this work, a large number of candidate networks (usually 1000) were trained starting with different initial network weights and biases, according to the Nguyen-Widrow scheme.[55] These networks were ranked based on their total performance

$$\varepsilon^{\text{overall}} = 0.8\varepsilon^{\text{training}} + 0.2\varepsilon^{\text{validation}}, \tag{5}$$

where $\varepsilon^{\text{training}}$ is the root mean square error (RMSE) of the training set, and $\varepsilon^{\text{validation}}$ is the RMSE of the validation set. Since the original database is divided in an 80/20 ratio, this is essentially the global RMSE of the neural network in predicting V^{NN} for all points in the database. We found that taking the 1% of 1000 candidate networks with the smallest error, ranked by $\varepsilon^{\text{overall}}$, gave MD results which were statistically insignificant from MD results coming from a larger number of candidate networks.

F. Novelty sampling

We used an iterative novelty sampling algorithm to obtain an accurate, converged PES. This approach was first implemented in the MS interpolation approach of Collins[10,11,24,25] and recently extended to systems using neural networks by Raff *et al.*[29] The basic algorithm used in this work is outlined in Fig. 2. We start with a small database of configurations and energies, much smaller than what is necessary to obtain an accurate parametrization of the PES. These seed configurations are chosen randomly, so that their center of mass falls within the parallelepiped that is defined by the 2×2 surface unit cell and 5 Å of vacuum above the surface. The bond length is chosen randomly between 0.5 and 3.0 Å, and the polar angle and azimuth of the H–H bond are also randomized. This corresponds to a random, uniform sampling of Cartesian space, which is in the range of MD simulations, translated into the primitive surface unit cell.

On this database, we train a large number of neural networks and choose the best ten of these networks based on $\varepsilon^{\text{overall}}$, and perform multiple MD simulations using all ten selected neural networks. During these MD simulations, configurations are periodically sampled and saved for a subsequent selection procedure. From these candidate configurations, several are selected in which the neural network has a high probability of predicting incorrectly. These configurations are then used as inputs to an *ab initio* technique, added to the database, and the process is started over. During the course of this algorithm a dynamic observable, such as the reaction probability at a given incident energy, is monitored for convergence. When this observable is invariant with respect to the number and density of configurations in the database, the process is halted.

Every iteration of the algorithm, we perform between 50 and 150 trajectories, which are intended to identify configurations that the neural network may predict incorrectly. For the first ten iterations of the novelty sampling scheme, we only grow the training set by 50 configurations each cycle, since the PES is not very accurate and there is a strong possibility of sampling unphysical configurations. From iterations 11–20, the PES becomes more accurate, and the number of configurations added to each cycle is increased to 100. From iteration 21–30, we add 150 configurations, etc.

These trajectories are split between the ten neural networks selected for MD (i.e., 5, 10, or 15 trajectories are run for each neural network in the top 1% of candidate networks). The initial conditions are randomized (see Sec. II A), and the trajectories are carried out at a random collision energy which is physically meaningful. For example, the collision energy range used for the H_2/Pt(111) system spanned from 0.5 to 13.0 kcal/mol, which corresponds to the range where reaction begins to take place and where all incident molecules react.[6,8] During each of these sample trajectories, the system's configuration is recorded every femtosecond, generating a set of K configurations and their associated transformed coordinates, $\bar{\mathbf{q}}_i$, $i=1,\ldots,K$. For each sampled point from the aforementioned trajectories, we identify its closest configuration in the training database, and assign it a numerical score based on how similar the sample configuration is to the closest database configuration. Letting L represent the number of configurations in our training database, we calculate a weighted L2 norm of the difference between transformed coordinates for each point i in our sample set

$$\lambda_i = W(\bar{\mathbf{q}}_i) \min_{j=1,\ldots,L} \|\bar{\mathbf{q}}_i - \mathbf{q}_j\|, \quad i = 1, \ldots, K, \tag{6}$$

where λ_i is the score of configuration i, $W(\bar{\mathbf{q}}_i)$ is a weighting factor, and $\mathbf{q}_j$ is the transformed coordinate of the jth configuration in the training database. Using Cartesian coordinates in the norm of Eq. (6) is not ideal, since a sampled configuration may be far away from a database configuration in real space, but similar to a mirror image of that configuration. By using transformed coordinates, we eliminate this problem since all mirror images have the same $\mathbf{q}$ vector. Also, the range of all seven terms in Eq. (3) is approximately

the same. The novelty score is therefore a measure of how similar a trajectory configuration was to a database configuration. A low score indicates that a sampled configuration, $\bar{\mathbf{q}}_i$, was similar to at least one entry in the training database ($\lambda_i = 0$ if a trajectory configuration is the same as a database configuration). A high score indicates that the sampled configuration was dissimilar from all of the entries in the training database.

The scores given by Eq. (6) are multiplied by a weighting factor, $W(\bar{\mathbf{q}}_i)$, so that certain regions of phase space can be sampled more densely than others. For example, one might want more configurations in the entrance channel due to an early barrier to dissociation. In this work, we found that $W(\bar{\mathbf{q}}_i)=1$, which corresponds to a uniform density in the transformed coordinate system, adequately converged dynamics. Empirical attempts at weighting different regions of configuration phase based on potential energies and bond lengths/COM heights [different two-dimensional (2D) regions of the elbow plot shown in Fig. 1] were unsuccessful in reducing the number of training points needed for a fully converged PES.

Once each sample configuration is assigned a score, they are then normalized so that their sum is unity

$$\Gamma_i = \frac{\lambda_i}{\sum_{i=1}^{K} \lambda_i}. \tag{7}$$

A novel configuration K^* is stochastically chosen from this set for subsequent study using an *ab initio* technique. This method is similar to the second of the three selection criteria used by Raff *et al.* to identify novel configurations.[29] We select a random number r in the range (0,1) and find configuration K^* so that

$$\sum_{i=1}^{K^*-1} \Gamma_i \leq r < \sum_{i=1}^{K^*} \Gamma_i. \tag{8}$$

Since configurations with higher scores have a higher probability of being selected, the process tends to select configurations which are the most dissimilar from the training set. The introduction of some randomness is very helpful during the early stages of the novelty sampling algorithm to avoid selection of configurations which are all dissimilar from the training database, but very similar to each other.

This selection process is repeated, adding one novelty configuration per trajectory, until the desired number of configurations per iteration of the novelty algorithm is obtained. More sophisticated sampling procedures, such as the multicriteria process used by Raff *et al.*, were not needed for the 6D PESs considered in this work.[29] A key advantage of using neural networks within this framework is the relative ease at which they handle the irregularly spaced configurations this approach tends to generate. With neural networks, adding or removing arbitrary configurations in the training database presents no difficulties.

III. RESULTS AND DISCUSSION

We provide three demonstrations of the neural network/novelty sampling approach. The first two examples, H_2/Pt(111) (Ref. 15) and H_2/Cu(111),[31] do not use energies from *ab initio* calculations directly, but instead use analytic potentials that were developed using DFT calculations. These potentials are corrugated LEPS potentials, as described for diatom-surface systems by McCreery and Wolken[56,57] and extended by Persson *et al.*[31] to include a more flexible modified Morse potential for diatomic interactions. The LEPS potential functions are based on very accurate pair potentials, which reproduce DFT energies well, and a small subset of the complete PES, such as energies along a minimum energy path during dissociation. While they exhibit the proper qualitative dynamical behavior, they are not globally accurate and are generally only capable of reproducing energies of the smaller subset on which they were trained. However, by using an analytic potential, the "exact" result of the MD simulations can be calculated, which allows a quantitative, absolute assessment of the convergence of the dynamics during the novelty sampling process. The final example is the H_2/Pt(111) system, but this time we use the energies obtained from DFT directly, instead of a LEPS potential. These results are compared to previous semiclassical trajectories which used a PES based on different exchange and correlation functionals.[21]

A. PT(111)-LEPS

For the first system we considered, H_2/Pt(111), we used a previously reported corrugated LEPS PES (Ref. 15) in the place of DFT calculations. This potential used Sato parameters[56,57] $\Delta_a = 0.2172$ and $\Delta_m = -0.1032$, which were selected to reproduce energies obtained from a nudged elastic band calculation along the minimum energy path for dissociative chemisorption of hydrogen over the top site on the surface. The diatomic potentials used were a slightly modified form of what was previously reported,[15] and can be found in Appendix A of this work.

Before attempting to use the novelty sampling scheme, we wanted to isolate and eliminate variations in the MD due to artifacts of neural network training. In order to do this, we created a large training database consisting of 4000 configurations and energies, where any errors due to incomplete training data should be minimized. Configurations for the training database were chosen at random, sampled uniformly from the parallelepiped formed by the 2×2 surface unit cell and a vector extending 5 Å normal to the surface into the vacuum region. Configurations were only included in the training database if the potential energy of a configuration was below a value 1 eV higher than that of an isolated gas-phase hydrogen molecule. For the hydrogen-platinum system, the sticking coefficient begins to saturate near normal collision energies of 0.5 eV. This cutoff in energy was used since potential energies higher than this are unattainable in our MD simulations due to conservation of energy [0.56 eV is the maximum kinetic energy we consider for the H_2/Pt(111) system]. We will refer to the subset of configuration space within this energy range as the "dynamically

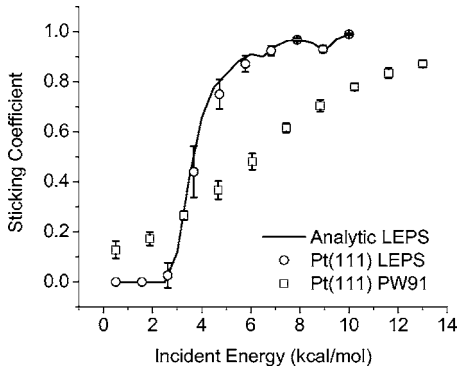

FIG. 3. Sticking coefficient as a function of incident energy for H_2/Pt(111) LEPS analytic potential, a neural network approximation of the LEPS potential, and a more accurate interpolated PES [Pt(111) PW91]. The solid line represents simulation results obtained using the LEPS potential directly, circles are the neural network approximation of the LEPS potential, and squares are results from the converged PES outlined in Sec. III C. Error bars are one standard deviation based on the ten best trainings of V^{NN}.

relevant" region. The reason for choosing a database in a random fashion, instead of on a regular grid, is that we found that off-grid configurations were predicted very poorly, the same conclusion reached by Lorenz *et al.*[28] using neural networks for the Pd(100) system. Only including highly symmetric configurations in our training database led to very large errors when a configuration not over a high symmetry site was presented to the network.

Figure 3 shows the results of MD simulations performed using the best ten fits from 1000 candidate networks, of 25-25-1 *stl* topology, on a database of 4000 random configurations in the dynamically relevant window. These sticking probabilities are compared to results obtained using the analytic potential directly, the exact result, and a globally accurate PES which we will discuss in Sec. III C. Despite having a small amount of scatter, the neural network representation of the analytic PES is very good. However, when compared to the globally accurate Pt(111) PW91 PES, the corrugated LEPS potential yields a reaction probability curve which is too narrow, and shifted to lower collision energies.

Each mark in Fig. 3 represents the results from a neural network ensemble—it is the average of the sticking coefficient predicted by the best trainings of the database of configurations. By averaging over several neural networks, we reduce the variability in MD due to errors in network training, and obtain an estimate of training errors.[58] The results shown in Fig. 3 indicate that with a database of configurations that was of proper density, the functional form outlined in Secs. II C–II E is at least capable of approximating a complex 6D corrugated LEPS potential. Very high levels of accuracy in network training were obtained. For this database, $\varepsilon^{\text{training}} < 5$ meV and $\varepsilon^{\text{validation}} < 10$ meV.

The key drawback to creating a configuration database for PES training in this manner is the very large number of configurations needed. The database held 4000 configurations, but these were only those configurations falling within the dynamically relevant region of phase space. When picking configurations for the H_2/Pt(111) LEPS system randomly, there is only a 20% chance of obtaining a configuration with an energy falling within this dynamically relevant

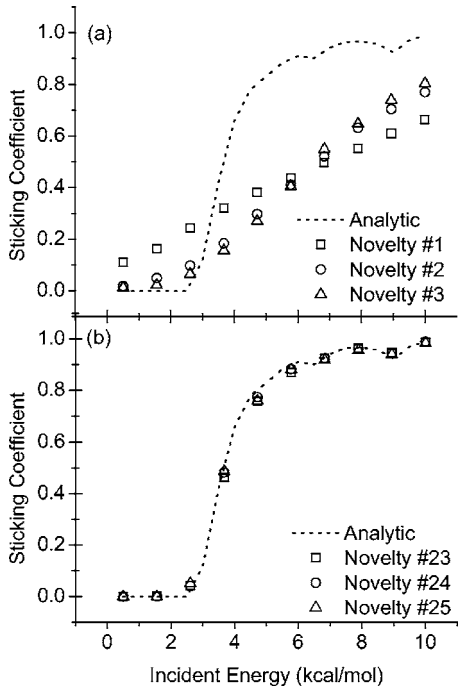

FIG. 4. Convergence of the sticking coefficient as a function of novelty iteration for the Pt(111)-LEPS system. Shown are (a) the first three iterations of the algorithm and (b) the last three iterations of the algorithm. Dotted line represents MD results obtained using analytic potential directly; marks are the average of ten neural networks approximating that analytic potential.

window. Most randomly selected configurations have energies which are too high—the position of the atoms is unphysical. Therefore, the total number of configurations that would need to be calculated using an *ab initio* technique to create a database of 4000 is 20 000. In addition to the large number of configurations not used in network training, it is also more difficult to converge the electronic structure of unphysical configurations in DFT, adding even more computational time. Eliminating this computational excess is one of the key motivating factors behind using the novelty sampling approach with an off-grid interpolation technique.

Having demonstrated the capabilities of the functional form, we next use the novelty sampling approach and grow a much smaller initial training database until an accuracy on par with that achieved for the 4000 random configurations case is obtained. The database was initialized with the first 500 configurations from the database of 4000 used earlier. During the first ten iterations of the novelty scheme outlined in Fig. 2, 50 configurations were added to the database per iteration, while for iterations 11–25, 100 configurations were added to the database every iteration. Any sampled points not falling within the dynamically relevant region were removed from the database. Figure 4 shows the sticking coefficient as a function of incident energy over the first three (a) and last three (b) iterations of the novelty algorithm, compared to analytic results. Each mark in Fig. 4 is the ensemble average of ten different estimates of s_0, each calculated using one of the ten different trainings of the neural network. Neural networks based on the initial 500 configurations, shown as novelty No. 1 in Fig. 4, give rise to potentials which are not very accurate and do not agree well with the analytic

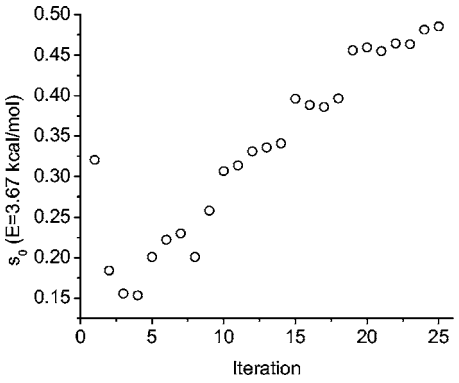

FIG. 5. Sticking coefficient of the H_2/Pt(111) LEPS system simulated at an incident energy of 3.67 kcal/mol as a function of novelty iteration.

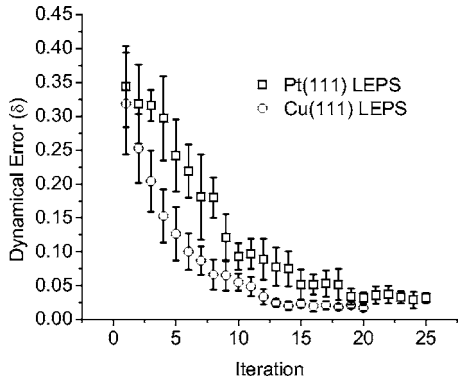

FIG. 6. Dynamical error (δ) as a function of iteration for the Pt(111) and Cu(111) LEPS PES. Error bars are one standard deviation based on ten different trainings of V^{NN} of the same database of configurations.

result. However, by the last three iterations of the algorithm, the neural network based PES is nearly identical to analytic results.

In order to show the convergence of the dynamics more clearly, the sticking coefficient at a single collision energy, $E=3.67$ kcal/mol, is shown as a function of iteration in Fig. 5. This incident energy was chosen so that the reaction probability was near one-half at the termination of the novelty sampling algorithm. It is clear from Fig. 5 that the sticking coefficient has approached a constant value during the last seven iterations, and the dynamics have converged. What is also interesting is that the values of sticking coefficient seem to be clustered as a function of iteration. It appears that every few iterations a new group of configurations is added to the database, which opens up a new reaction channel that the MD simulations begin exploring. As a more numerical assessment of dynamic convergence, we calculate the dynamical error, which is the RMSE between the sticking probability calculated using the analytic potential and the neural network's approximation of that potential

$$\delta = \sqrt{\frac{\sum_{i=1}^{N_E}(s_{0i}^{\mathrm{NN}} - s_{0i}^{\mathrm{LEPS}})^2}{N_E}}, \tag{9}$$

where δ is the dynamical error, N_E is the number of discrete incident energies where the neural network was used to estimate the sticking coefficient, s_{0i}^{NN} is the sticking coefficient calculated using the neural network as a potential function at incident energy E_i, and s_{0i}^{LEPS} is the sticking coefficient calculated using the LEPS potential directly. For all MD simulations reported in this work, $N_E=10$. This is the RMSE between the marks shown in Fig. 4 and the dotted line representing the analytic potential. δ is plotted as a function of iteration for the H_2/Pt(111) LEPS system in Fig. 6. The error gradually falls as a function of iteration, approaching zero as the number of iterations increases. Empirically choosing a cutoff δ value of 0.05 as a stopping criterion, the novelty algorithm converged at iteration 19. What is also interesting is that the overall dynamic error does not follow the "clustering" of the single incident energy. The energy chosen for Fig. 5 is in a region of the sticking curve where ds_0/dE is large (the sticking probability is most sensitive to PES changes) and is therefore very sensitive to changes in the training database.

During this entire process, all sampled configurations identified by the novelty scheme had energies falling within the dynamically relevant window. The novelty sampling scheme is therefore an excellent "generating function," providing very good initial guesses for future configurations to include in the database, even while the dynamics may be far from converged. By iteration 19, the database held 1850 configurations, the first 500 of which were generated by searching random configurations. Since there is only a 20% chance of finding a random configuration within the dynamically relevant region, it would take five times that number, or 2500 trial *ab initio* calculations, to generate the seed database of 500 configurations. The total number of "theoretical" DFT calculations needed to generate the entire database at iteration 19, if we were using an *ab initio* technique instead of an analytic potential, is therefore 3850. This is only 19% of the number of configurations needed when we created the entire database randomly, a tremendous savings if electronic structure calculations are the slowest step in generating a PES.

While it is easy to assess the absolute convergence of dynamics directly when using an analytic potential, it is impossible when using an *ab initio* technique since the exact dynamic result is not known. We therefore look at the convergence of three nondynamic metrics, based only on information available from the potential function and the configurations in the database. Figure 7(a) shows the root mean square error and root median square error of the network's measurement residual. The measurement residual is defined as the difference between the neural network's prediction of a novelty configuration's potential energy, and the correct potential energy determined by an *ab initio* technique (or in this case, the LEPS potential). The reason for showing both the mean and median will be addressed in Sec. III C, for now they both can be considered good moments of the distribution of measurement residuals. As the size of the database grows, the neural network becomes better at predicting the energies of the sampled novelty configurations. By the very end of the algorithm, the prediction error of new configurations approaches 5 meV (0.11 kcal/mol), the same accuracy at which the potential predicts the training database.

Another nondynamical statistic is the average novelty score $\bar{\lambda}$,

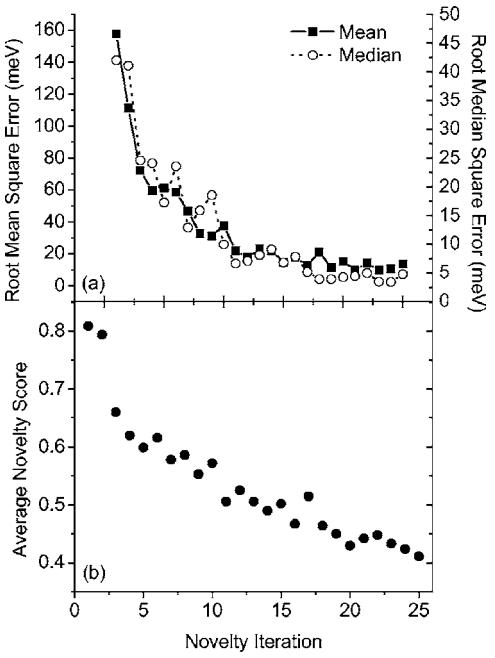

FIG. 7. Convergence of nondynamical statistics as a function of novelty iteration for the H_2/Pt(111) LEPS system. (a) Root mean square error and root median square error of each iteration's measurement residual. (b) Convergence of the average novelty score as a function of iteration.

$$\bar{\lambda} = \frac{1}{N_N}\sum_{i=1}^{N_N} \lambda(\mathbf{q}_i^{K^*}), \tag{10}$$

where N_N is the number of novelty points added to the training database of each iteration (50, 100, or 150 depending on which iteration) and $\lambda(\mathbf{q}_i^{K^*})$, $i=1,\ldots,N_N$ represents the novelty score [Eq. (6)] of the selected configurations. The convergence of $\bar{\lambda}$ is shown as a function of novelty iteration in Fig. 7(b). This statistic, which measures how dissimilar the novelty configurations are from the database, is only based on the position of configurations and not their energies. This quantity exhibits an almost linear decline during advancement of the algorithm, and has a value of 0.46 at iteration 19 when the dynamics have converged.

B. Cu(111)-LEPS

As a second test of the novelty sampling algorithm, we extended the approach to the H_2/Cu(111) system, modeled using a corrugated LEPS potential developed by Persson *et al.*[31] for Eley-Rideal reactions of H with a H covered Cu(111) surface. This system is a nice complement to the H_2/Pt(111) system because it is highly activated along all reaction channels and the sticking coefficient exhibits activity over a much wider range of incident energies. As with the H_2/Pt(111) system, the novelty sampling scheme was started with a database of 500 configurations. The database was grown 50 configurations per iteration of the novelty sampling scheme during the first ten configurations, and 100 configurations during iterations 11–20. A key difference between this system and the hydrogen-platinum system is that the dynamically relevant window is much larger, extending 2.5 eV above the isolated gas-phase hydrogen potential energy. This is due to the fact that the collision energy range over which the H_2/Cu(111) system saturates is much wider and shifted to higher energies. Other than this difference in energetics, the approach and analysis for this system were identical to the H_2/Pt(111) LEPS system.

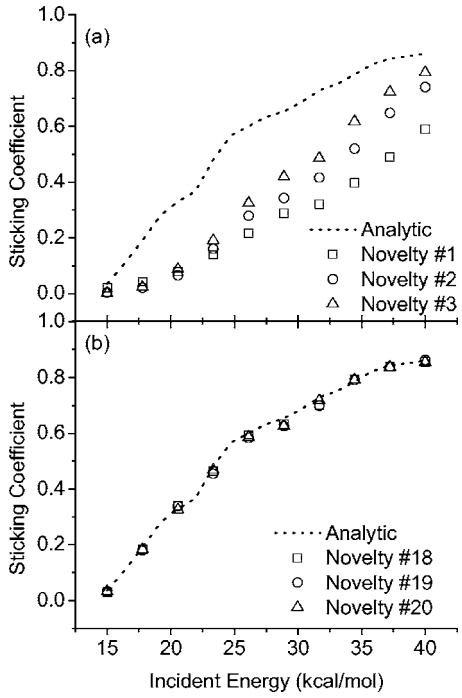

FIG. 8. Convergence of the sticking coefficient as a function of novelty iteration for the Cu(111)-LEPS system. Shown are (a) the first three iterations of the algorithm and (b) the last three iterations of the algorithm. Dotted line represents MD results obtained from using the analytic potential directly; marks are neural network approximation of that analytic potential.

Figure 8 shows the convergence of the sticking coefficient for the first three (a) and last three (b) iterations of the novelty algorithm. Again, the analytic solution is shown along with the neural network approximation to demonstrate convergence of the dynamics. As with the platinum-hydrogen system, the initial PESs are not very good, but rapidly improve as the training database grows. The sticking coefficient as a function of novelty iteration at a single incident energy, $E=23.3$ kcal/mol, is shown in Fig. 9. The sticking coefficient is relatively constant over the last eight iterations of the novelty scheme. The convergence of the

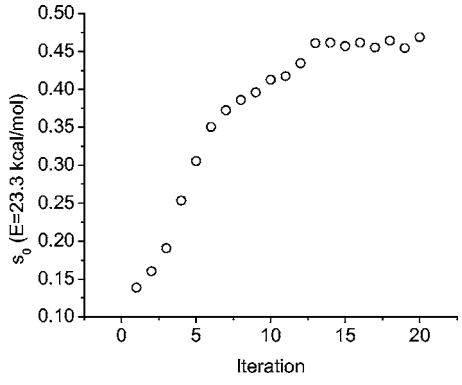

FIG. 9. Sticking coefficient of the H_2/Cu(111) LEPS system simulated at an incident energy of 23.3 kcal/mol as a function of novelty iteration.

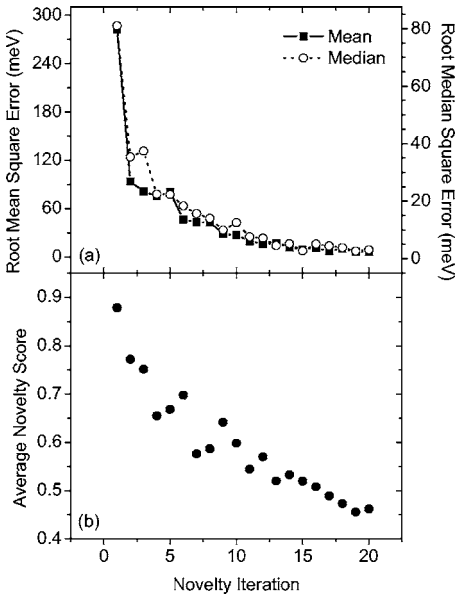

FIG. 10. Convergence of nondynamical statistics as a function of novelty iteration for the H_2/Cu(111) LEPS system. (a) Root mean square error and root median square error of each iteration's measurement residual. (b) Convergence of the average novelty score as a function of iteration.

dynamical error δ is shown as a function of iteration against the H_2/Pt(111) LEPS system in Fig. 6. Using the same cutoff value of $\delta=0.05$, we find that this system converges at iteration 11, with 1050 configurations in the database.

The fact that the H_2/Cu(111) LEPS PES converges with almost half the number of configurations in the database as the H_2/Pt(111) LEPS PES is a direct result of the higher activation barriers in the hydrogen-copper system. With a small activation barrier along the minimum energy path, and a minimal amount of energetic corrugation over the surface, trajectories will follow multiple pathways from reactants to products. With more channels to dissociation available, more information about the PES is needed in a wider subset of configuration space. As the PES becomes more activated, the number of configurations relevant to dynamics begins to shrink as the number of accessible reaction channels begins decreasing. Transition state theory can be thought of as a limit of this process—during a highly activated process all reactive trajectories must pass through a unique saddle point in the PES, the transition state. It is therefore no surprise that the H_2/Pt(111) LEPS system converges more slowly than the H_2/Cu(111) LEPS system.

The convergence of the same nondynamic observables shown for the hydrogen-platinum system, i.e., the measurement residual and the novelty score, is shown for the hydrogen-copper system in Fig. 10. All nondynamic indicators more or less monotonically decrease as a function of iteration. As with the platinum system, a final RMSE measurement residual of 5 meV is attained, which is the same as the training set.

One outstanding issue before we move on the final example using *ab initio* energies directly is that of the uniqueness of the potential. It is clear that the novelty sampling process should converge, but it is not clear that it should converge to a globally accurate PES. In order to find reaction channels that the potential has no knowledge of, it must explore somewhere near them during the novelty sampling process. If this does not occur, it is entirely possible to obtain a converged potential, which is not globally valid. In this case, the final converged PES can be viewed as a function of the initial "seed" database. To a certain extent, inclusion of enough initial random configurations should mitigate this issue, but it is impossible to ensure this. It is reassuring that for two very dissimilar systems the potential did, in fact, converge to give dynamics in agreement with what we know to be correct, but we would like to point out that this is in no way guaranteed.

C. Pt(111)-PW91

As a final example demonstrating the novelty sampling approach, we used DFT to calculate potential energies directly, instead of using an analytic potential. As with the previous systems, we initialized the training database with 500 random configurations, each configuration having a potential energy falling within the dynamically relevant region. This energy window was the same as it was for the H_2/Pt(111) LEPS system, with a cutoff of 1 eV above the potential energy of a hydrogen molecule in the gas phase. In contrast to the H_2/Pt(111) and H_2/Cu(111) LEPS systems, the neural network size was allowed to vary as a function of novelty algorithm iteration. This was necessary since it was unknown at the start of the novelty sampling process exactly how many configurations would be needed to accurately capture the dynamics. Every ten iterations, training was attempted with a network size of five neurons larger and smaller in each layer, and a new network size was chosen based on the results of a *t*-test on $\varepsilon^{\text{overall}}$ for the ten best networks. The final network topology at the termination of the novelty algorithm for this system was 50-50-1 *stl*, significantly larger than the network size needed for the analytic potentials. This larger size is expected, since the true 6D *ab initio* PES should have more corrugation and complexity than the LEPS approximation of it.

In Fig. 11, we show the convergence of the sticking coefficient as a function of incident energy for the (a) first three and (b) last three iterations of the algorithm. Also shown in Fig. 11 are experimental molecular beam data from Luntz *et al.*[6] and Samson *et al.*,[8] along with results from the aforementioned semiclassical trajectories performed by Pijper *et al.*[21] A comparison with the LEPS is shown in Fig. 3. Despite the experimental results of Luntz *et al.* being for D_2/Pt(111), no isotope effect was detected either experimentally[6] or theoretically[22] so that a direct comparison is possible. The dynamic results obtained from running trajectories on a PES trained on only the first 500 configurations give sticking probabilities which are in very good agreement with experimental results. However, it must be stressed that at this point in the novelty algorithm the agreement is fortuitous. Validation errors ($\varepsilon^{\text{validation}}$) over the first three iterations all exceed 150 meV, indicating a poor global description of the PES. The 95% confidence interval of s_0 in the first iteration is ±12.8%, which is due to large differences between the ten networks used to generate the sticking curve.

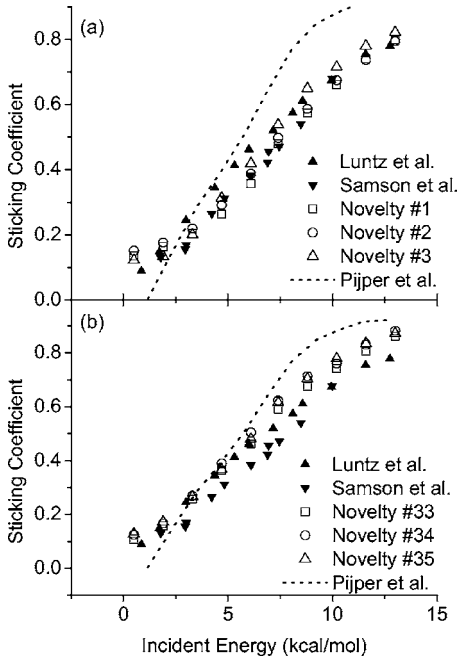

FIG. 11. Convergence of the sticking coefficient as a function of novelty iteration for the Pt(111)-PW91 system. Shown are (a) the first three iterations of the algorithm and (b) the last three iterations of the algorithm. Open marks are simulation results; filled marks are molecular beam experiments from Luntz *et al.* (Ref. 6) and Samson *et al.* (Ref. 8). Dotted line is previous semiclassical MD results of Pijper *et al.* using CRP potential (Ref. 21).

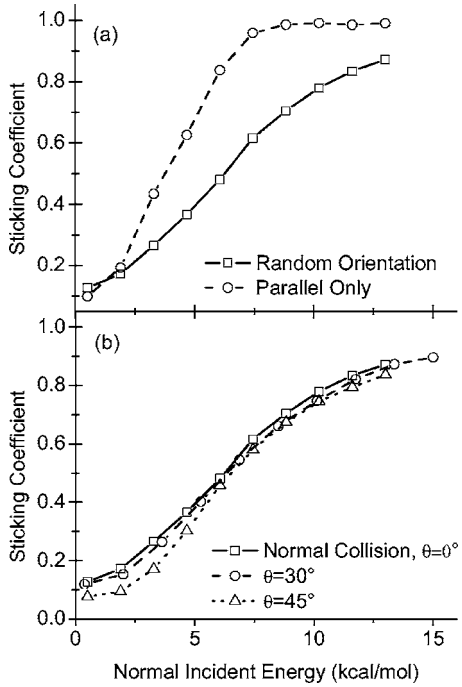

FIG. 12. (a) Sticking coefficient as a function of incident energy for randomly oriented initial configurations vs those where the H–H bond vector was initially constrained to be parallel to the surface. (b) The effect of impact angle, the angle of the initial velocity vector makes with the surface normal, on sticking coefficient. The crystallographic direction along which trajectories were performed was randomized.

As the algorithm progresses, the entire sticking curve begins to shift to higher values, closer to the theoretical results obtained by Pijper *et al.*[21] However, the final sticking curve obtained using the PW91 functional is not drastically different than the one from the first iteration and is in better overall agreement with experiments than previous semiclassical and quantum dynamics results.[20–22]

Vincent *et al.*[22] explored many of the potential sources of the discrepancy between the quantum dynamics results of Pijper *et al.*[20,21] and experiments. Effects studied included isotope effects, phonons, initial rotational distributions, and energy dispersion in the incident beam. All of these issues were investigated to see if they could explain the fact that the simulations were predicting a narrower reaction probability curve than what was measured experimentally. They concluded that none of these effects would cause significant broadening of the reaction curve and that intrinsic features of the potential energy surface were to blame. They hypothesize that the generalized gradient approximation used (Becke[59] for exchange and Perdew[60] for correlation) gave a distribution of reaction barriers that was too narrow, which in turn gave rise to dynamics that occurred over a narrow range of incident energies. Specifically, they calculated the minimum and maximum barriers to dissociation for configurations with the H–H bond held fixed parallel to the surface and find a barrier of 0.06 eV dissociation over the top site and 0.42 eV over the fcc hollow site.[20]

The average barriers calculated for identical dissociation sites using our PES for the last iteration are 0.06 eV for the top site and 0.33 eV for the fcc site. Despite our PES exhibiting less energetic corrugation for configurations where the bond is held parallel to the surface, we still obtain a wider reaction curve. The lack of energetic corrugation with the PW91 functional was also seen in the H_2/Ru(0001) (Refs. 61 and 62) system, when compared to non-self-consistent RPBE results.[38] However, although the PW91 functional generated a PES with less energetic corrugation, it had greater geometric corrugation. A more detailed description of various dissociation pathways is given in Appendix B and Fig. 15, where we describe six 2D slices of our converged PES that can be compared directly to those published by Olsen *et al.*[17]

In order to understand which of these effects, energetic or geometric corrugation, was most prominent in our system, we performed trajectories where the initial conditions were chosen so that the H–H bond was oriented parallel to the surface. Results from these trajectories are compared to those obtained by a randomization of the initial H–H azimuth in Fig. 12(a). Restricted in this manner, the reaction probability curve becomes narrower and shifts to lower energies, consistent with the energetic corrugation seen for this orientation. The reaction probability saturates near an incident energy of 7.5 kcal/mol (0.33 eV), which corresponds to the maximum reaction barrier seen for parallel orientations. Because of this, and taking into account results from the H_2/Ru(0001) system, we believe that the wider reaction curve is a result of geometric corrugation. That is, either reaction pathways where the H–H bond is not parallel to the surface play a significant role in the dissociation dynamics or steering effects are more prominent in our PES. There are also other significant differences in the underlying quantum mechanical treatment that may contribute to dynamical differences. In our DFT calculations, in addition to using a different ex-

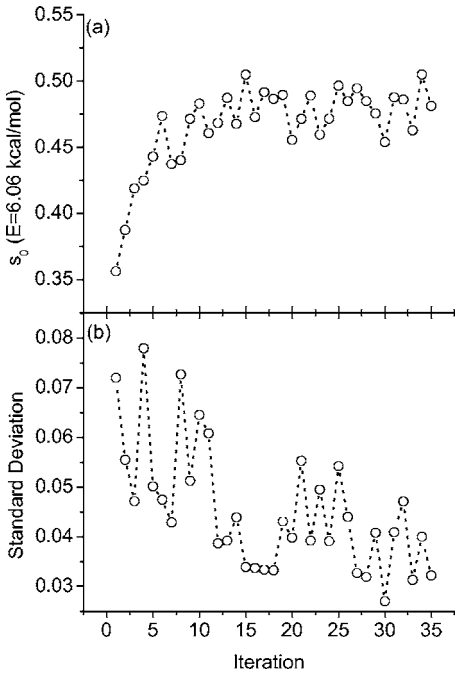

FIG. 13. (a) Sticking coefficient of the H_2/Pt(111) PW91 system simulated at an incident energy of 6.06 kcal/mol as a function of novelty iteration. (b) Standard deviation of s_0 at E=6.06 kcal/mol based on ten neural networks as a function of iteration.

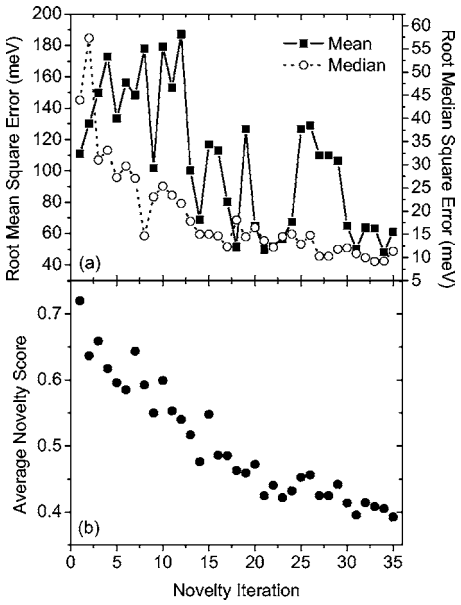

FIG. 14. Convergence of nondynamical statistics as a function of novelty iteration for the H_2/Pt(111) PW91 system. (a) Root mean square error and root median square error of each iteration's measurement residual. (b) Convergence of the average novelty score as a function of iteration.

change and correlation functional, the platinum slab had four layers, a relaxed lattice constant, and a pseudopotential treatment was used for the core electrons. It is unclear how important each of these effects may be, since we would need to develop a separate PES varying each assumption to deconvolute these sources of error.

As with the LEPS surfaces, we find it helpful to monitor the sticking coefficient at a fixed incident energy as a function of iteration. The convergence of s_0 for E =6.06 kcal/mol is shown as a function of iteration in Fig. 13(a). Starting at a value of s_0 near 0.35, the sticking probability climbs to an average value of s_0=0.475 toward the end of the algorithm. Compared to the H_2/Pt(111) LEPS case, there is a significant amount of scatter in the reaction probability as a function of iteration, reflecting the greater difficulty in training and representing a true *ab initio* database as opposed to a much smoother analytic potential. However, the fluctuations seen after iteration 15 are not very large and would be acceptable for purposes of parameter estimation in microkinetic models or other engineering purposes.

In Fig. 13(b), we show the convergence of the standard deviation of the sticking coefficient as a function of novelty iteration. This value, calculated from ten different trainings of the neural network, is a measure of how much variability in s_0 can be attributed to network training errors. As the database grows in size, this value shrinks, indicating that training errors, which are differences between neural networks trained on the same database, become less significant as the density of configurations in the database rises. If we were to use the results shown in Fig. 13 as a basis for convergence, it would appear that additional configurations after iteration 15 did not significantly alter dynamic results. At this iteration, the database had 1436 configurations, which is approximately half the number of points needed to obtain an accurate representation using the CRP.[10,11] However, when the initial 2500 configurations needed for the initial seed database are included, we required approximately the same number of configurations as Crespos *et al.*[10,11] using the modified Shepard approach (~3000). However, in our approach one does not need to calculate second derivatives, which adds significant computational time to the modified Shepard approach. Using AMD Opteron 246 processors, the entire novelty sampling process for the H_2/Pt(111) system, including neural network training and DFT calculations, took approximately 10 processor years to complete (or roughly 3 months on a 40 processor Beowulf cluster). The Hessian calculation needed by the MS technique would add significantly to this development time.

The convergence of nondynamic observables as a function of iteration is shown in Fig. 14. Compared to the H_2/Pt(111) LEPS and H_2/Cu(111) LEPS systems, the root mean square error of the measurement residuals shows erratic fluctuations as a function of iteration. This is due to the presence of outliers in the measurement residual. Out of the 50 or 100 new novelty configurations added to the database per iteration, the measurement residual of one or two configurations can be very high. Most of these outliers occurred with configurations that were very close to the surface and having extended H–H bonds. In this region of configuration space, the potential should be behaving like two independent pair potentials [$V^{\mathrm{H-H}}$ and V^{NN} should tend to zero in Eq. (2)]. Because of this, we suspect that errors in the atom-surface pair potentials, $V^{\mathrm{Pt\text{-}1}}$ and $V^{\mathrm{Pt\text{-}2}}$, cause these outliers. These issues do not occur in the two previous examples using analytic potentials since the LEPS potential takes the pair potentials as input[31,56,57] and therefore these terms are exact.

If the atom-surface interactions are even slightly incorrect, V^{NN} does not tend to zero in the limit of a dissociated

TABLE I. **H** matrix for H/Pt(111) system.

	m_1	m_2	m_3	m_4	m_5
d	2.665	-3.25×10^{-2}	-8.65×10^{-3}	1.24×10^{-2}	8.35×10^{-3}
z_0	1.270	1.78×10^{-1}	-2.04×10^{-4}	-1.60×10^{-2}	-7.46×10^{-3}
a	1.263	1.48×10^{-1}	3.17×10^{-3}	-5.27×10^{-2}	-3.08×10^{-2}
$\tilde{a}$	0.794	1.43×10^{-2}	-1.71×10^{-3}	1.89×10^{-2}	1.29×10^{-2}
z_1	2.239	3.19×10^{-2}	9.29×10^{-4}	-1.55×10^{-2}	-9.03×10^{-3}
β	4.000	-2.55×10^{-20}	-5.57×10^{-21}	-1.48×10^{-16}	4.25×10^{-21}

configuration, since V^{NN} must also account for errors in the pair potential. This causes network training to become more difficult, which is reflected in the larger network size needed during training and higher values of $\varepsilon^{\mathrm{training}}$ as compared to network training using analytic potentials. Every effort should therefore be made to ensure that the pair-additive potentials in a CRP-like approach are as accurate as possible. Despite having an occasional outlier problem, we note that the average measurement residual is a worse-case statistic of the performance of the neural network. These are precisely the configurations the neural network has identified as problematic—other configurations are predicted much more accurately. By the last iteration of the novelty algorithm, the database had 3860 configurations with $\varepsilon^{\mathrm{training}}=17$ meV, or roughly 0.4 kcal/mol. This value compares well with the accuracy of 30 meV, reported by Pijper *et al.* as the maximum error in the barrier region of the CRP potential.[20] Also outliers occurred only with specific trainings of the neural network. We believe that using an ensemble of many networks for a given training database effectively mitigates this issue. Therefore, for the H_2/Pt(111) PW91 system, we monitor the root median square error as a function of iteration, instead of the RMSE, since the median is less sensitive to outliers than the mean. As the algorithm converges, this value approaches 10 meV (0.23 kcal/mol), which indicates a very accurate prediction of the energies of most new configurations identified by the novelty sampling procedure (the outliers being the exception to this).

As a final test of our converged potential, we investigate a well known dynamic feature of the H_2/Pt(111) system—the non-normal scaling of sticking coefficient with collision energy.[6,19,20] The sticking coefficient as a function of impact angle (θ) and normal incident energy ($E_\perp = E\cos^2\theta$) is presented in Fig. 12(b). Impact angle is defined as the angle the initial velocity vector makes with the surface normal at the start of the trajectory. If parallel momentum had no effect on sticking, the curves shown in Fig. 12(b) would overlap. Instead we see an inhibition of sticking at low collision energies, which increases with increasing incidence angle. This effect, caused by energetic corrugation in the PES, has previously been reported for H_2/Pt(111) (Refs. 19 and 20) and other model systems.[63,64] As our goal with this work is the demonstration of an algorithm for PES refinement, we refer readers to those sources for a rigorous physical explanation of this effect. We show these results only to demonstrate that despite being trained on novelty configurations coming from normal collisions ($\theta=0$), the PES is potentially globally accurate and captures the proper qualitative behavior when parallel momentum is added to our simulations. A proper description of dynamics involving parallel momentum is extremely important, as it indicates that extrapolation of these simulations to initial conditions taken from a Maxwell distribution is possible. This suggests a procedure where a PES is qualified against molecular beam experiments, and then extrapolated to conditions that are more representative of those encountered in heterogeneous catalysis.

IV. CONCLUSIONS

We outlined a hybrid approach to developing potential energy surfaces for diatom-surface reactions, which results in semiclassical MD simulations that are converged with respect to DFT. This algorithm uses a modified version of the corrugation reduction procedure,[23] neural networks as interpolating functions for a residual term in the PES,[27–30,33,41–51] and a novelty sampling procedure which couples MD to the quantum mechanical calculations needed for an accurate parametrization of configuration space.[10,11,24,25,29] Starting with a seed database of random configurations, which have potential energies relevant to MD, we grew the database until MD simulations converged. This was first done for two systems, H_2/Pt(111) (Ref. 15) and H_2/Cu(111),[31] using analytic potentials, which were based on DFT, in the place of direct quantum mechanical calculations. Not only did this reduce the time to complete the novelty sampling algorithm, it allowed a numerical assessment of dynamical convergence since the "exact" results of the MD simulations were known *a priori*. Compared to the H_2/Pt(111) system, the highly activated H_2/Cu(111) system converged much more rapidly as a function of iteration of the novelty sampling. With higher activation barriers, the number of reaction channels in the copper system was smaller than that of the platinum system, and therefore the volume of configuration space explored by trajectories was smaller. This in turn led to a more rapid convergence of MD simulations since the number of configurations having an ultimate impact on dynamics was smaller.

As a final example of the technique, the H_2/Pt(111) system was revisited and DFT, with the PW91 (Ref. 32) exchange and correlation functionals, was used to obtain potential energies for the training database directly. MD simulations performed using this PES were compared to previous semiclassical trajectories[21] which used a PES based on a different set of exchange and correlation functionals. Using the final converged PES, which had $\varepsilon^{\mathrm{training}}=17$ meV, we found that our system exhibited a broader reaction probabil-

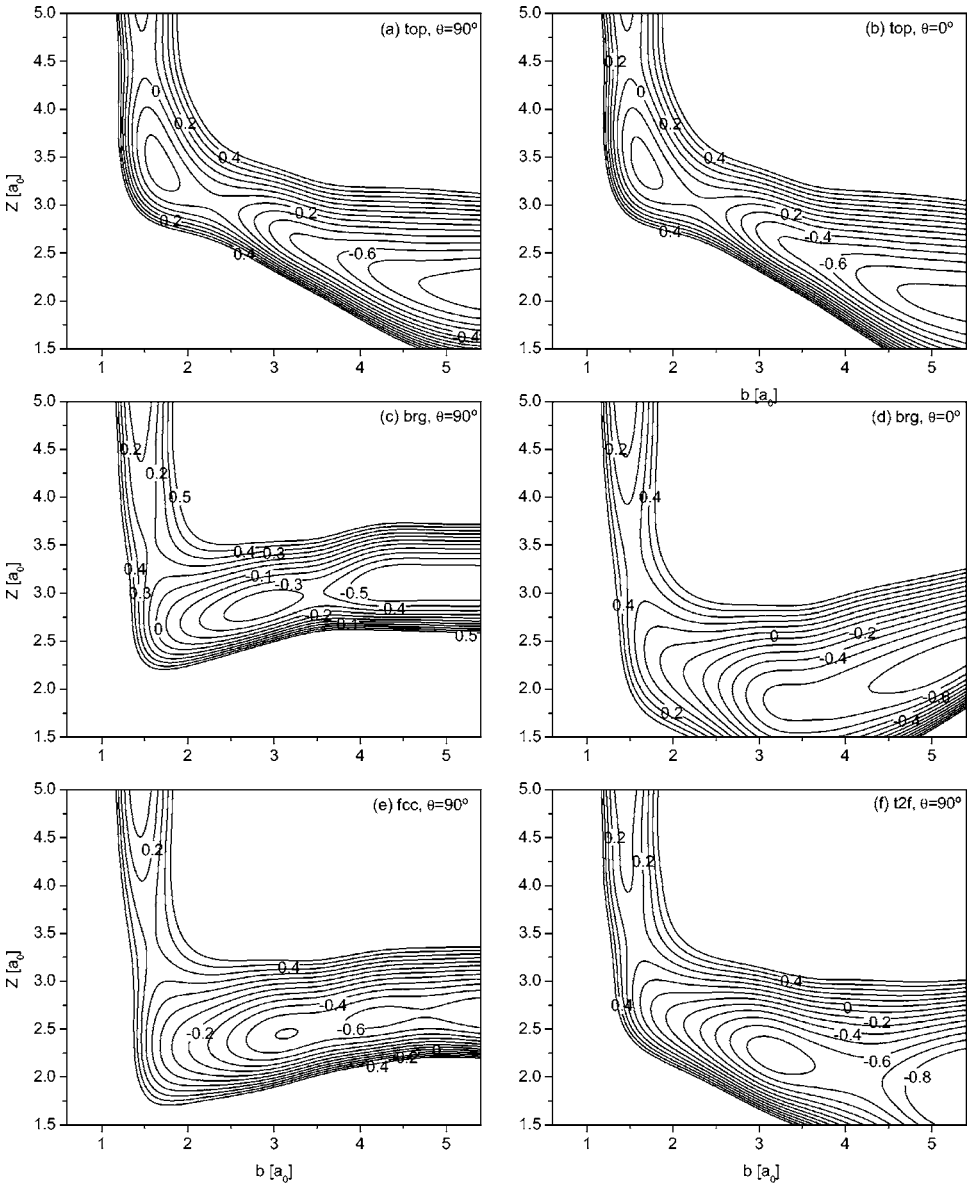

FIG. 15. Two dimensional cuts of the converged PES for the H_2/Pt(111) system over six different dissociation sites. The H–H bond (b) was taken to be parallel to the surface, with the bond vector making an angle θ with the ⟨110⟩ direction of the Pt(111) surface. The COM of the H_2 molecule was centered over one of the six sites shown in Fig. 1 of Ref. 17, the height of the COM above the surface is given by Z. The potential energy was taken with the H_2 molecule in the gas phase as a reference, units are in a.u., and spacing of contour lines is 0.1 eV. This was done to be consistent with the 2D slices shown in Fig. 5 of Ref. 17.

ity curve, in better agreement with experiment than previous simulations, despite having a lower energetic corrugation. We attribute this difference to geometric corrugation in the PES which causes nonparallel dissociation pathways to become important. Finally, we show that for H_2/Pt(111), normal energy scaling is not obeyed, in agreement with previous simulations and experiments. Despite only being trained on trajectories resulting from normal collisions, off-normal dynamics are captured accurately. This indicates that the PES has a chance of accurately predicting trajectories where the initial conditions come from a Maxwell distribution, allowing prediction of kinetic parameters useful in microkinetic modeling research.

The goal of this work was to demonstrate an approach to PES construction which is a hybrid of some of the outstanding features of recent work.[23,24,27–29] We recognize that more accurate dynamics simulations, specifically 6D quantum dynamics simulations, may be necessary to reproduce experimental data, or even capture the correct qualitative behavior. However, even if the ultimate goal is quantum dynamics, semiclassical mechanics serve as a good "generating function" of configurations for subsequent *ab initio* methods. Even trained on a very small database of configurations, semiclassical MD simulations explore physically sound configurations and seldom recommend a configuration which is too high in energy to be of no practical use to dynamics. We feel that neural networks used in combination with a symmetry adapted coordinate system, novelty sampling, and the CRP are an excellent tool for creating highly accurate diatom-surface potentials. This approach can drastically reduce the computational cost and time associated with PES development, and provides some assurance that the PES is accurate.

ACKNOWLEDGMENTS

We acknowledge partial support of this research by the U.S. Department of Energy, under Award No. DE-FG02-03ER15468. However, any opinions, findings, conclusions, or recommendations expressed herein are those of the authors and do not necessarily reflect the views of the DOE. The authors would like to thank Professor Douglas Doren,

for helpful discussions regarding the use of neural networks as interpolating functions for potential energy surfaces, and Professor Babatunde Ogunnaike, for helpful discussion regarding statistical methods used to assess convergence.

APPENDIX A: ATOM-SURFACE POTENTIAL

There are two different types of pair potentials described in Eq. (2). Both of these pair potentials use the modified Morse form described by Persson *et al.*,[31]

$$V^{\text{pair}}(z) = d(\exp[-2a(z-z_0)] - 2f(z)\exp[-a(z-z_0)]),$$
$$f(z) = \exp\left(\frac{\tilde{a}(z-z_0)}{1+\exp(-\beta a(z-z_1))}\right), \tag{A1}$$

where V^{pair} is the potential energy, z is either the distance between the two hydrogen atoms (for the H–H pair) or the perpendicular distance between a hydrogen and the surface (for the H–Pt pair), and $f(z)$ is a switching function. d, z_0, a, $\tilde{a}$, z_1, and β are adjustable parameters.

For the case of the H–H pair potential, these parameters are constants and adjusted to reproduce the potential energy of a hydrogen molecule as a function of bond length. These values are given in Ref. 15. For the H–Pt pair potential, these parameters are functions of the atom's projection onto the surface (x-y position). This is done by expanding these parameters in a truncated Fourier series, similar to that of Eq. (3),

$$[d\ z_0\ a\ \tilde{a}\ z_1\ \beta]^{\mathrm{T}} = \mathbf{Hm},$$
$$\mathbf{m} = \begin{bmatrix} \cos(2\alpha y/\sqrt{3}) + 2\cos(\alpha x)\cos(\alpha y/\sqrt{3}) \\ \sin(2\alpha y/\sqrt{3}) - 2\cos(\alpha x)\sin(\alpha y/\sqrt{3}) \\ \cos(2\alpha x) + 2\cos(\alpha x)\cos(\sqrt{3}\alpha y) \\ 2\cos(2\alpha x)\cos(2\alpha y/\sqrt{3}) + \cos(4\alpha y/\sqrt{3}) \end{bmatrix}, \tag{A2}$$

where $\mathbf{H}$ is a matrix of adjustable coefficients, which is multiplied by vector $\mathbf{m}$, which has elements that are terms of a Fourier expansion in 2D with C_{3v} symmetry. α is given by Eq. (4). This forces each of the six adjustable Morse potentials to have the correct symmetry and be periodic functions of the x-y location over the surface. For more details on this approach, see works by Persson *et al.*[31] and Busnengo *et al.*[23] The coefficients used in this work can be found in Table I, which we adjust to reproduce DFT results from six different locations on the surface.

APPENDIX B: 2D PES SLICES

Six 2D slices of the converged PES for the Pt(111)-PW91 system are given in Fig. 15. Each of the cuts was obtained by averaging the potential from each of the ten networks, which made up the converged ensemble of networks. These cuts were taken to be identical to those of Olsen *et al.*,[17] allowing a direct comparison of PESs. Interestingly, both dissociation channels over the top site show a shallow molecular well in the PES. Dissociation over all other surface sites shows lower barriers than those calculated by Olsen *et al.*[17] However, the sticking coefficient is a function of all dissociation channels, not just those where the H–H bond is held parallel to the surface. This makes drawing conclusions based on a limited number of 2D slices difficult.

[1] G. R. Darling and S. Holloway, Rep. Prog. Phys. **58**, 1595 (1995).
[2] A. Gross, Surf. Sci. Rep. **32**, 291 (1998).
[3] G. J. Kroes, Prog. Surf. Sci. **60**, 1 (1999).
[4] M. Bonn, A. W. Kleyn, and G. J. Kroes, Surf. Sci. **500**, 475 (2002).
[5] J. P. Cowin, C. F. Yu, S. J. Sibener, and L. Wharton, J. Chem. Phys. **79**, 3537 (1983).
[6] A. C. Luntz, J. K. Brown, and M. D. Williams, J. Chem. Phys. **93**, 5240 (1990).
[7] P. Nieto, E. Pijper, D. Barredo, G. Laurent, R. A. Olsen, E. J. Baerends, G. J. Kroes, and D. Farias, Science **312**, 86 (2006).
[8] P. Samson, A. Nesbitt, B. E. Koel, and A. Hodgson, J. Chem. Phys. **109**, 3255 (1998).
[9] N. B. Arboleda, H. Kasai, W. A. Dino, and H. Nakanishi, Thin Solid Films **509**, 227 (2006).
[10] C. Crespos, M. A. Collins, E. Pijper, and G. J. Kroes, Chem. Phys. Lett. **376**, 566 (2003).
[11] C. Crespos, M. A. Collins, E. Pijper, and G. J. Kroes, J. Chem. Phys. **120**, 2392 (2004).
[12] C. Crespos, H.-D. Meyer, R. C. Mowrey, and G. J. Kroes, J. Chem. Phys. **124**, 074706 (2006).
[13] S. M. Kingma, M. F. Somers, E. Pijper, G. J. Kroes, R. A. Olsen, and E. J. Baerends, J. Chem. Phys. **118**, 4190 (2003).
[14] G. J. Kroes and M. F. Somers, J. Theor. Comput. Chem. **4**, 493 (2005).
[15] J. Ludwig and D. G. Vlachos, Mol. Simul. **30**, 765 (2004).
[16] R. A. Olsen, H. F. Busnengo, A. Salin, M. F. Somers, G. J. Kroes, and E. J. Baerends, J. Chem. Phys. **116**, 3841 (2002).
[17] R. A. Olsen, G. J. Kroes, and E. J. Baerends, J. Chem. Phys. **111**, 11155 (1999).
[18] E. Pijper, G. J. Kroes, R. A. Olsen, and E. J. Baerends, J. Chem. Phys. **113**, 8300 (2000).
[19] E. Pijper, G. J. Kroes, R. A. Olsen, and E. J. Baerends, J. Chem. Phys. **116**, 9435 (2002).
[20] E. Pijper, G. J. Kroes, R. A. Olsen, and E. J. Baerends, J. Chem. Phys. **117**, 5885 (2002).
[21] E. Pijper, M. F. Somers, G. J. Kroes, R. A. Olsen, E. J. Baerends, H. F. Busnengo, A. Salin, and D. Lemoine, Chem. Phys. Lett. **347**, 277 (2001).
[22] J. K. Vincent, R. A. Olsen, G. J. Kroes, and E. J. Baerends, Surf. Sci. **573**, 433 (2004).
[23] H. F. Busnengo, A. Salin, and W. Dong, J. Chem. Phys. **112**, 7641 (2000).
[24] M. A. Collins, Theor. Chem. Acc. **108**, 313 (2002).
[25] J. Ischtwan and M. A. Collins, J. Chem. Phys. **100**, 8080 (1994).
[26] C. Diaz, J. K. Vincent, G. P. Krishnamohan, R. A. Olsen, G. J. Kroes, K. Honkala, and J. K. Norskov, Phys. Rev. Lett. **96**, 096102 (2006).
[27] S. Lorenz, A. Gross, and M. Scheffler, Chem. Phys. Lett. **395**, 210 (2004).
[28] S. Lorenz, M. Scheffler, and A. Gross, Phys. Rev. B **73**, 115431 (2006).
[29] L. M. Raff, M. Malshe, M. Hagan, D. I. Doughan, M. G. Rockley, and R. Komanduri, J. Chem. Phys. **122**, 084104 (2005).
[30] P. M. Agrawal, L. M. Raff, M. T. Hagan, and R. Komanduri, J. Chem. Phys. **124**, 134306 (2006).
[31] M. Persson, J. Stromquist, L. Bengtsson, B. Jackson, D. V. Shalashilin, and B. Hammer, J. Chem. Phys. **110**, 2240 (1999).
[32] J. P. Perdew, in *Electronic Structure of Solids '91*, edited by P. Ziesche and H. Eschrig (Akademie, Berlin, 1991).
[33] T. B. Blank, S. D. Brown, A. W. Calhoun, and D. J. Doren, J. Chem. Phys. **103**, 4129 (1995).
[34] D. A. McCormack, R. A. Olsen, and E. J. Baerends, J. Chem. Phys. **122**, 194708 (2005).
[35] M. P. Allen and D. J. Tildesley, *Computer Simulation of Liquids* (Oxford University Press, New York, 1987).
[36] A. Agresti and B. A. Coull, Am. Stat. **52**, 119 (1998).
[37] B. Hammer, O. H. Nielsen, J. J. Mortensen, L. Bengtsson, L. B. Hansen, A. C. E. Madsen, Y. Morikawa, T. Bligaard, and A. Christensen, DACAPO 2.7, Technical University of Denmark, Lyngby, Denmark, 2003.
[38] B. Hammer, L. B. Hansen, and J. K. Norskov, Phys. Rev. B **59**, 7413 (1999).
[39] D. Vanderbilt, Phys. Rev. B **41**, 7892 (1990).
[40] H. J. Monkhorst and J. D. Pack, Phys. Rev. B **13**, 5188 (1976).

[41] A. C. P. Bittencourt, F. V. Prudente, and J. D. M. Vianna, Chem. Phys. **297**, 153 (2004).
[42] D. F. R. Brown, M. N. Gibbs, and D. C. Clary, J. Chem. Phys. **105**, 7597 (1996).
[43] K. H. Cho, K. T. No, and H. A. Scheraga, J. Mol. Struct. **641**, 77 (2002).
[44] D. I. Doughan, L. M. Raff, M. G. Rockley, M. Hagan, P. M. Agrawal, and R. Komanduri, J. Chem. Phys. **124**, 054321 (2006).
[45] H. Gassner, M. Probst, A. Lauenstein, and K. Hermansson, J. Phys. Chem. A **102**, 4596 (1998).
[46] S. Manzhos and T. Carrington, J. Chem. Phys. **125**, 084109 (2006).
[47] S. Manzhos, X. Wang, R. Dawes, and T. Carrington, Jr., J. Phys. Chem. A **110**, 5295 (2006).
[48] F. V. Prudente, P. H. Acioli, and J. J. S. Neto, J. Chem. Phys. **109**, 8801 (1998).
[49] F. V. Prudente and J. J. S. Neto, Chem. Phys. Lett. **287**, 585 (1998).
[50] T. M. Rocha, Z. T. Oliveira, L. A. C. Malbouisson, R. Gargano, and J. J. S. Neto, Int. J. Quantum Chem. **95**, 281 (2003).
[51] J. B. Witkoskie and D. J. Doren, J. Chem. Theory Comput. **1**, 14 (2005).
[52] H. Demuth, M. Beale, and M. Hagan, *Neural Network Toolbox User's Guide*, 9th ed. (Unknown Binding, Natick, MA, 2005).
[53] D. W. Marquardt, J. Soc. Ind. Appl. Math. **11**, 431 (1963).
[54] W. S. Sarle, "Stopped training and other remedies for over-fitting," presented at the Proceedings of the 27th Symposium on the Interface of Computing Science and Statistics (1995), p. 352.
[55] D. Nguyen and B. Widrow, IEEE Control Syst. Mag. **3**, 18 (1990).
[56] J. H. McCreery and G. Wolken, Jr., J. Chem. Phys. **63**, 2340 (1975).
[57] J. H. McCreery and G. Wolken, Jr., J. Chem. Phys. **67**, 2551 (1977).
[58] L. K. Hansen and P. Salamon, IEEE Trans. Pattern Anal. Mach. Intell. **12**, 993 (1990).
[59] A. D. Becke, Phys. Rev. A **38**, 3098 (1988).
[60] J. P. Perdew, Phys. Rev. B **33**, 8822 (1986).
[61] M. Luppi, R. A. Olsen, and E. J. Baerends, Phys. Chem. Chem. Phys. **8**, 688 (2006).
[62] J. K. Vincent, R. A. Olsen, G. J. Kroes, M. Luppi, and E. J. Baerends, J. Chem. Phys. **122**, 044701 (2005).
[63] G. R. Darling and S. Holloway, Surf. Sci. **304**, L461 (1994).
[64] A. Gross, J. Chem. Phys. **102**, 5045 (1995).